Supporting Information

Exchange-Driven Slow Relaxation of Magnetization in $Ni^{II}_2Ln^{III}_2$ (Ln^{III} = Y, Gd, Tb and Dy) Butterfly complexes: Experimental and Theoretical Studies

Amit Chakraborty,* [a, b †] Naushad Ahmed,[a †] Shruti Moorthy[c], Joydeb Goura,[d] Saurabh Kumar Singh* [c], Guillaume Rogez* [d], Vadapalli Chandrasekhar* [a d]

[a] *Tata Institute of Fundamental Research, 36/P, Gopanpally Village, Serilingampally Mandal, Ranga Reddy District, Hyderabad 500046.*

[b] *Department of Chemistry, Inorganic Chemistry Section, Jadavpur University, Kolkata 700032, India.*

[c] *Department of Chemistry, Indian Institute of Technology Hyderabad, Kandi-502285, Sangareddy,Telangana, India.*

[d] *Department of Chemistry, IIT Kanpur, Kanpur 208016, India.*

[e] *Institut de Physique et Chimie des Matériaux de Strasbourg, UMR 7504 CNRS-Université de Strasbourg, 23 rue du Loess, B.P. 43, 67034 Strasbourg Cedex 2, France*

Supporting Information

Table S1. Crystallographic parameters for complexes **1-4**.

Compound	**1**	**2**	**3**	**4**
CCDC Number	2120514	2120087	2120513	2120086
Empirical formula	$C_{54}H_{56}N_6Ni_2O_{18}Y_2$	$C_{54}H_{56}Gd_2N_6Ni_2O_{18}$	$C_{54}H_{56}N_6Ni_2O_{18}Tb_2$	$C_{54}H_{56}Dy_2N_6Ni_2O_{18}$
Formula weight ($gmol^{-1}$)	1372.25	1508.93	1512.29	1519.43
Temperature (K)	100(2)	100(2)	100(2)	100 (2)
Crystal system	orthorhombic	orthorhombic	orthorhombic	orthorhombic
Space group	Pbcn	Pbcn	Pbcn	Pbcn
Unit cell lengths (Å)	a= 15.0051(7) b = 24.3858(10) c = 14.8468(8)	a = 14.939(5) b = 24.343(5) c = 14.845(5)	a = 14.824(3) b = 24.353(5) c = 14.610(3)	a = 14.952(5) b = 24.363(5) c = 14.825(5)
Unit cell angles (°)	α= 90 β = 90 γ = 90	α = 90.000(5) β = 90.000(5) γ = 90.000(5)	α = 90.000(5) β = 90.000(5) γ = 90.000(5)	α = 90.000(5) β = 90.000(5) γ = 90.000(5)
Volume ($Å^3$)	5432.6(4)	5399(3)	5275(2)	5400(3)
Z	4	4	4	4
Density (calculated)	1.678	1.856	1.905	1.869
Absorption coefficient	2.879	3.193	3.435	3.504
F(000)	2800.0	3000.0	3008.0	3016.0
Crystal size (mm)	0.18 × 0.16 × 0.14	0.25 × 0.23 × 0.21	0.24 × 0.22 × 0.20	0.16 × 0.15 × 0.14
2θ range for data collection (°)	5.43 to 58.062	5.454 to 50.994	3.216 to 50.996	5.114 to 51
Reflections collected	59843	20805	27129	20908
Index ranges	-20 ≤ h ≤ 19, -32 ≤ k ≤ 32, -15 ≤ l ≤ 20	-14 ≤ h ≤ 18, -29 ≤ k ≤ 23, -17 ≤ l ≤ 16	-17 ≤ h ≤ 15, -29 ≤ k ≤ 29, -11 ≤ l ≤ 17	-18 ≤ h ≤ 15, -24 ≤ k ≤ 29, -17 ≤ l ≤ 17
Independent reflections	6699 [R_{int} = 0.1332]	4962 [R_{int} = 0.0574]	4915 [R_{int} = 0.0735]	4804 [R_{int} = 0.1044]
Data/Restrain/Parameter	6699/3/379	4962/0/380	4915/2/379	4804/0/380
Goodness-of-fit on F^2	1.023	1.029	1.075	0.985
Final R indices [I>2sigma(I)]	R_1 = 0.0464, wR_2 = 0.0995	R_1 = 0.0379, wR_2 = 0.0727	R_1 = 0.0457, wR_2 = 0.1042	R_1 = 0.0476, wR_2 = 0.0596
R indices (all data)	R_1 = 0.0820, wR_2 = 0.1108	R_1 = 0.0931, wR_2 = 0.0869	R_1 = 0.0683, wR_2 = 0.1168	R_1 = 0.1542, wR_2 = 0.0791

Supporting Information

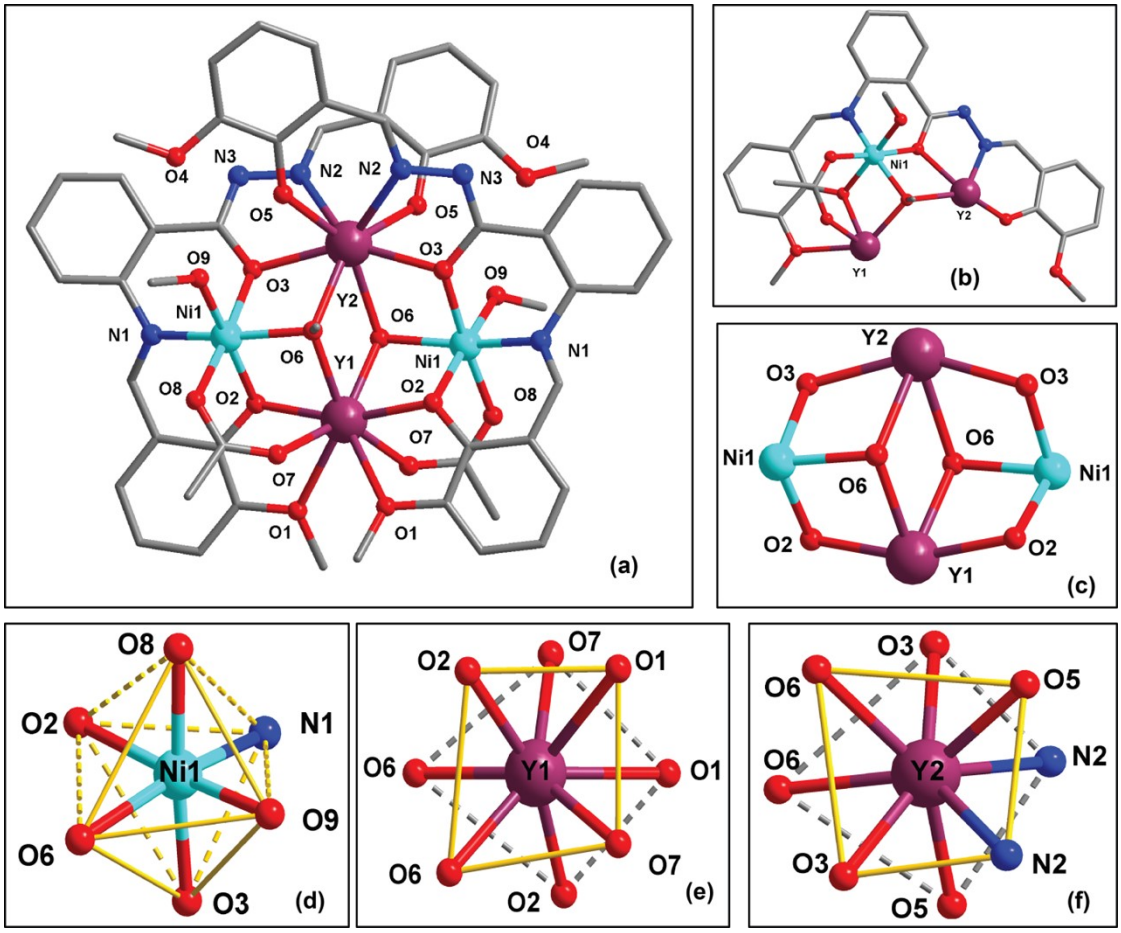

Figure S1. Crystal structure of complex **1** (a) asymmetric unit present in the lattice (b) butterfly arrangement of Ni_2Y_2 core (c).

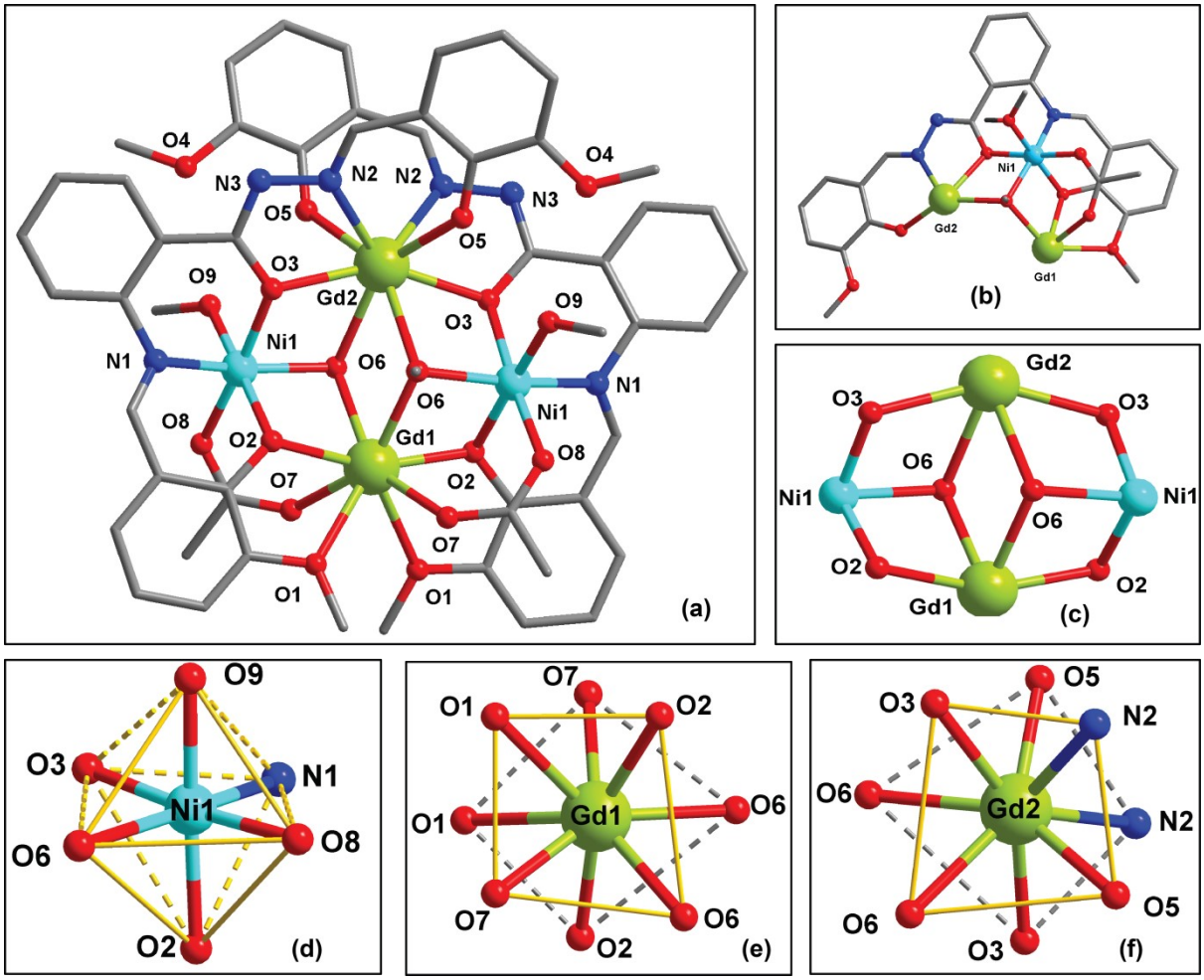

Figure S2. Crystal structure of complex **2** (a) asymmetric unit present in the lattice (b) butterfly arrangement of Ni_2Gd_2 core (c).

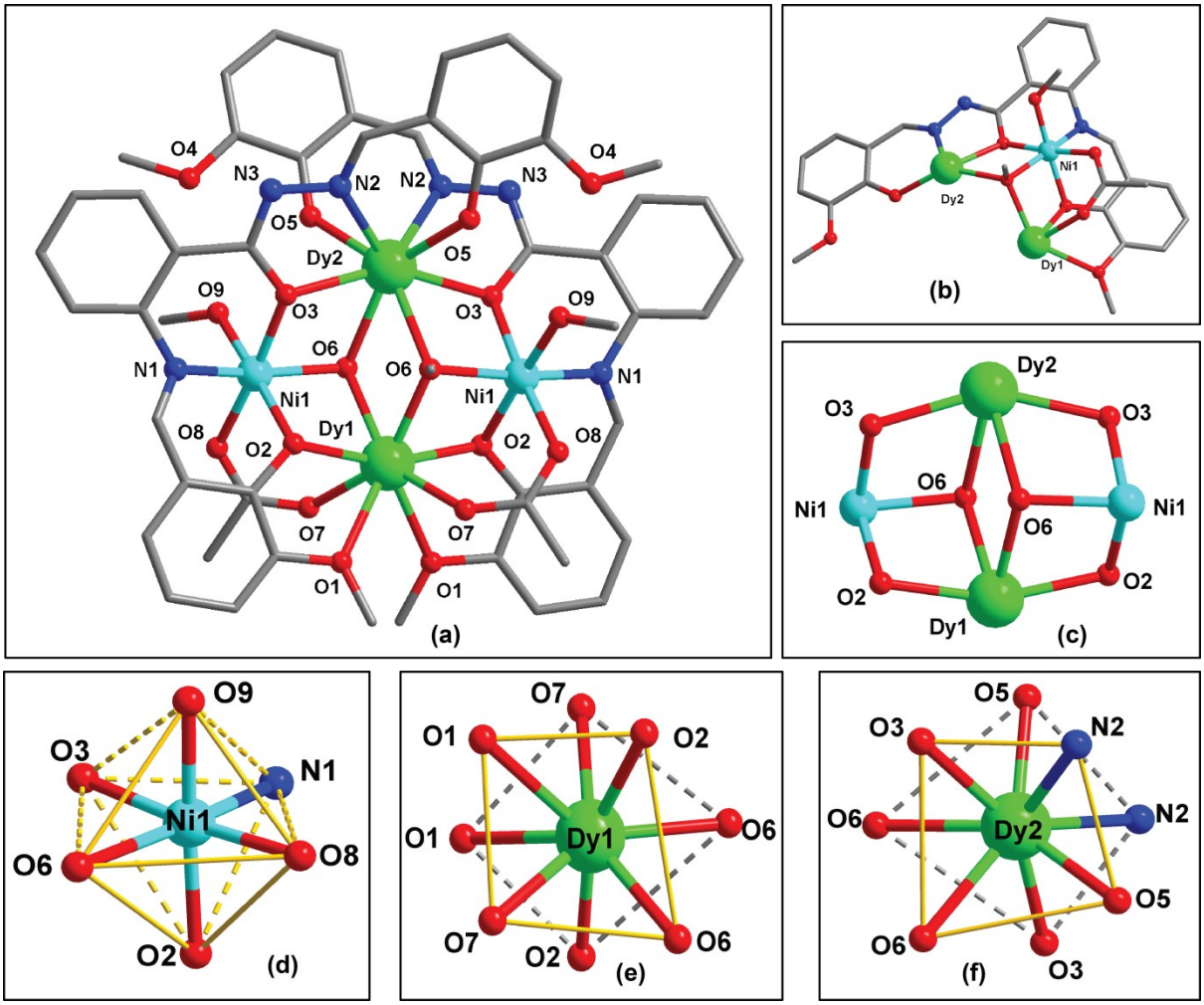

Figure S3. Crystal structure of complex **4** (a) asymmetric unit present in the lattice (b) butterfly arrangement of Ni_2Dy_2 core (c).

Supporting Information

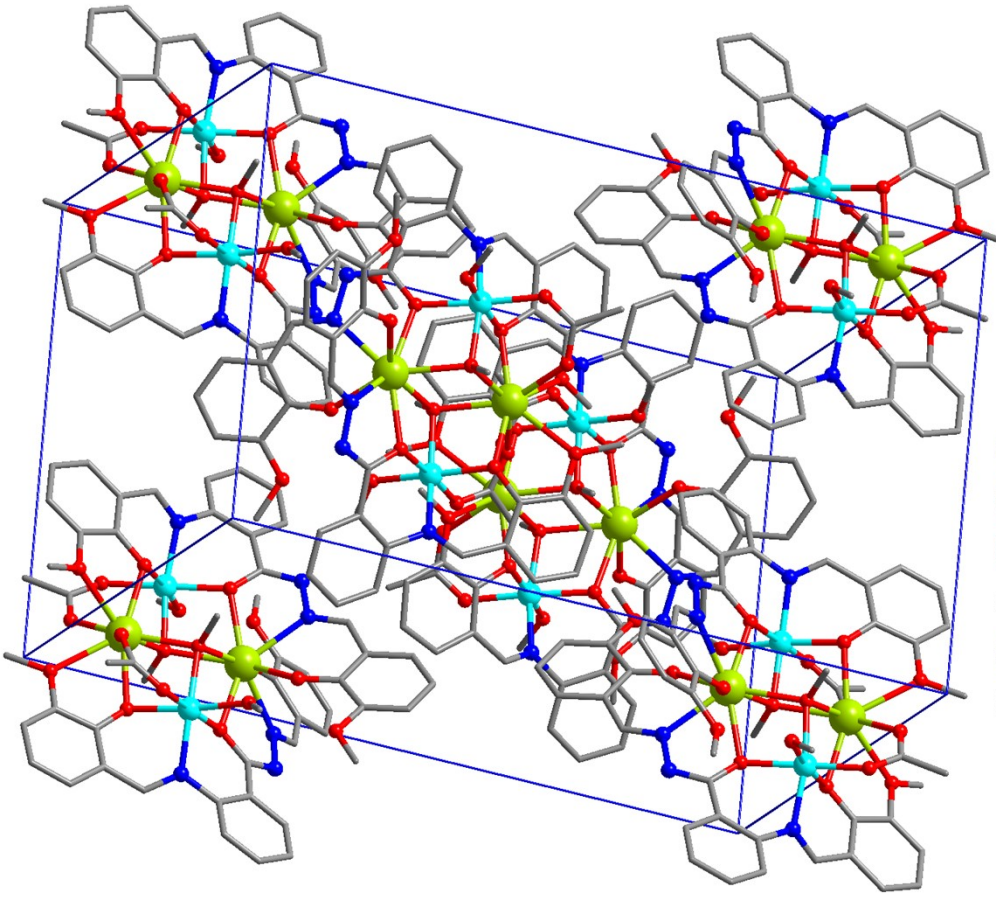

Figure S4. Packing structure for representative complex **3** along the c-axis.

Table S2. Possible geometries around the Ln(III) metal centres and their corresponding CShM values.

	OP-8	HPY-8	HBPY-8	CU-8	SAPR-8	TDD-8	JGBF-8	JETBPY-8	JBTPR-8	BTPR-8	JSD-8	TT-8	ETBPY-8
Complex 1													
Y1	27.380	23.129	16.919	11.547	**1.217**	2.433	12.023	24.888	2.557	2.437	3.522	12.381	19.672
Y2	27.423	22.754	15.116	10.923	**2.086**	4.077	13.772	20.585	4.802	4.131	7.061	11.290	15.113
Complex 2													
Gd1	27.122	23.223	17.265	11.861	**1.200**	2.439	12.473	24.060	2.726	2.520	3.823	12.085	18.759
Gd2	27.742	22.624	14.985	10.936	**2.349**	4.233	13.664	20.061	5.099	4.360	7.373	11.296	14.550
Complex 3													
Tb1	26.957	23.387	17.429	12.022	**1.193**	1.193	12.295	24.172	2.671	2.459	3.725	12.274	18.943
Tb2	27.082	22.602	15.211	11.073	**2.166**	4.299	13.747	20.292	4.819	4.272	7.003	11.424	14.782
Complex 4													
Dy1	27.382	23.157	17.138	11.840	**1.281**	2.392	11.956	24.576	2.614	2.476	3.544	12.366	19.293
Dy2	27.163	22.579	15.201	11.089	**2.209**	4.265	13.729	20.166	4.920	4.272	7.164	11.464	14.714

OP-8, D_{8h}, Octagon; **HPY-8**, C_{7v}, Heptagonal pyramid; **HBPY-8**, D_{6h}, Hexagonal bipyramid; **CU-8**, O_h, Cube; **SAPR-8**, D_{4d}, Square antiprism; **TDD-8**, D_{2d},Triangular dodecahedron; **JGBF-8**, D_{2d}, Johnson gyrobifastigium J26; **JETBPY-8**, D_{3h}, Johnson elongated triangular bipyramid J14; **JBTPR-8**, C_{2v}, Biaugmented trigonal prism J50; **BTPR-8**, C_{2v}, Biaugmented trigonal prism; **JSD-8**, D_{2d}, Snub diphenoid J84; **TT-8**, T_d , Triakis tetrahedron; **ETBPY**-8, D_{3h}, Elongated trigonal bipyramid.

Supporting Information

Table S3. Bond lengths and bond angles in complex **1**

Bond lengths (Å)	Bond lengths (Å)	Bond angles (°)
Y2-O6, 2.4487(18)	Y1-O2*, 2.309(2)	Ni1-Y1-Y2, 56.545(8)
Y2-O61, 2.4487(18)	Y1-O2, 2.309(2)	Ni1*-Y1-Y2, 56.545(8)
Y2-O31, 2.3894(19)	Y1-O1, 2.577(2)	Ni1-Y1-Ni1*, 113.090(16)
Y2-O3, 2.3895(19)	Y1-O1*, 2.577(2)	Ni1*-Y2-Y1, 50.996(7)
Y2-O5*, 2.3303(18)	Y1-O7*, 2.293(2)	Ni1-Y2-Y1, 50.995(7)
Y2-O5, 2.3303(18)	Y1-O7, 2.293(2)	Ni1-Y2-Ni1*, 101.991(14)
Y2-N2, 2.469(2)	Ni1-O6, 2.109(2)	Y1-Ni1-Y2, 72.460(10)
Y2-N2*, 2.469(2)	Ni1-O3, 2.0304(18)	Y1-O6-Y2, 113.93(8)
Y1-Ni1*, 3.2758(4)	Ni1-O2, 2.091(2)	Ni1-O6-Y2, 100.74(7)
Y1-Ni1, 3.2758(4)	Ni1-O8, 2.047(2)	Ni1-O6-Y1, 94.53(7)
Y1-O6*, 2.3453(18)	Ni1-O9, 2.029(2)	Ni1-O3-Y2, 105.16(8)
Y1-O6, 2.3454(18)	Ni1-N1, 2.045(3)	Ni1-O2-Y1, 96.09(8)
	Y2-Y1, 4.0194(5) Y2-Ni1, 3.5170(4) Y2-Ni11, 3.5170(4)	

Table S4. Bond lengths and bond angles in complex **2**

Bond lengths (Å)	Bond lengths (Å)	Bond angles (°)
Gd1-Gd2, 4.0613(10)	Gd1-O7*, 2.337(4)	Ni1-Gd1-Gd2, 56.275(16)
Gd1-Ni1*, 3.3143(10)	Gd2-O6*, 2.477(3)	Ni1*-Gd1-Gd2, 56.274(16)
Gd1-Ni1, 3.3143(10)	Gd2-O6, 2.477(3)	Ni1-Gd1-Ni1* , 112.55(3)
Gd1-O6, 12.367(3)	Gd2-O5, 2.354(4)	Gd1-O6-Gd2 113.92(14)
Gd1-O6, 2.367(3)	Gd2-O5*, 2.354(4)	Ni1-O6-Gd1, 95.64(13)
Gd1-O1, 2.590(4)	Gd2-O3, 2.421(3)	Ni1-O6-Gd2 101.04(13)
Gd1-O1*, 2.591(4)	Gd2-O3*, 2.421(3)	Ni1-O3-Gd2, 104.85(14)
Gd1-O2, 2.350(4)	Gd2-N2*, 2.496(4)	Ni1-O2-Gd1, 96.65(14)
Gd1-O2*, 2.350(4)	Gd2-N2, 2.496(4)	
Gd1-O7, 2.337(4)	Ni1-O6, 2.099(4)	

	Ni1-O3, 2.036(3) Ni1-O2, 2.080(4) Ni1-O9, 2.038(4) Ni1-O8, 2.052(4) Ni1-N1, 2.044(5)	

Table S5. Bond lengths and bond angles in complex **3**

Bond lengths (Å)		Bond lengths (Å)		Bond angles (°)	
Tb1-O6*,	2.355(4)	Tb2-O5,	2.347(4)	Ni1*-Tb1-Ni1,	112.60(3)
Tb1-O6,	2.355(4)	Tb2-O3*	2.402(4)	Tb1-O6-Tb2,	113.97(18)
Tb1-O7,	2.321(4)	Tb2-O3,	2.402(4)	Ni1-O6-Tb1,	95.82(16)
Tb1-O7*,	2.321(4)	Tb2-N2*,	2.481(5)	Ni1-O6-Tb2,	100.97(16)
Tb1-O1*,	2.569(4)	Tb2-N2,	2.481(5)	Ni1-O2-Tb1,	96.85(16)
Tb1-O1,	2.570(4)	Ni1-O6,	2.097(4)	Ni1-O3-Tb2,	105.09(17)
Tb1-O2*,	2.338(4)	Ni1-O8*,	2.060(4)		
Tb1-O2,	2.338(4)	Ni1-O2,	2.078(4)		
Tb2-O6,	2.468(4)	Ni1-O3,	2.036(4)		
Tb2-O6*,	2.468(4)	Ni1-O9,	2.029(4)		
Tb2-O5*,	2.347(4)	Ni1-N1,	2.043(5)		
		Tb1-Ni1,	3.3084(9)		
		Tb1-Ni1*,	3.3083(9)		

Table S6. Bond lengths and bond angles in complex **4**

Bond lengths (Å)	Bond lengths (Å)	Bond angles (°)
Dy2-O6*, 2.455(4)	Dy1-O6*, 2.342(4)	Dy1-O6-Dy2, 114.40(17)
Dy2-O6, 2.455(4)	Dy1-O6, 2.342(4)	Ni1-O6-Dy2, 101.27(17)
Dy2-N2*, 2.467(6)	Dy1-O1, 2.585(5)	Ni1-O6-Dy1, 95.47(16)
Dy2-N2, 2.467(6)	Dy1-O1*, 2.585(5)	

Supporting Information

Dy2-O5, 2.332(5) Dy2-O5*, 2.332(5) Dy2-O3*, 2.399(4) Dy2-O3, 2.399(4) Dy1-Ni1*, 3.2871(12) Dy1-Ni1, 3.2871(11) Dy1-O2, 2.317(4) Dy1-O2*, 2.317(4)	Dy1-O7*, 2.297(6) Dy1-O7, 2.297(6) Ni1-O6, 2.094(4) Ni1-O3, 2.027(4) Ni1-O8, 2.048(5) Ni1-O9, 2.039(7) Ni1-O2*, 2.092(5) Ni1-N1, 2.042(6)	Ni1-Dy1-Ni1*, 112.93(4) Ni1-O3-Dy2, 105.25(19) Ni11-O2-Dy1, 96.28(18)

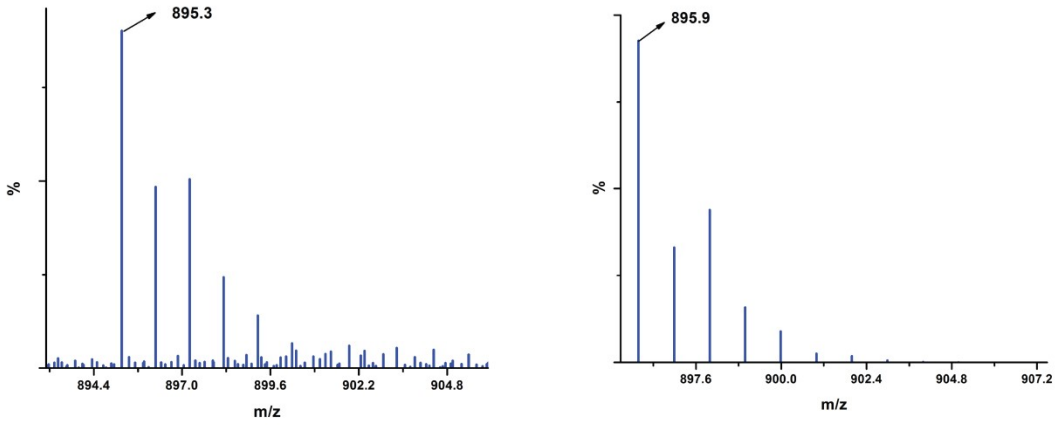

(a) (b)

Supporting Information

ESI-MS for complex **1**, detecting $[\{L'\{Ni(MeOH)(\mu\text{-}OAc)_2(\mu_3\text{-}MeO)_2Y_2\}\cdot(MeOH)]^+$ fragment, (a) experimental and (b) theoretical.

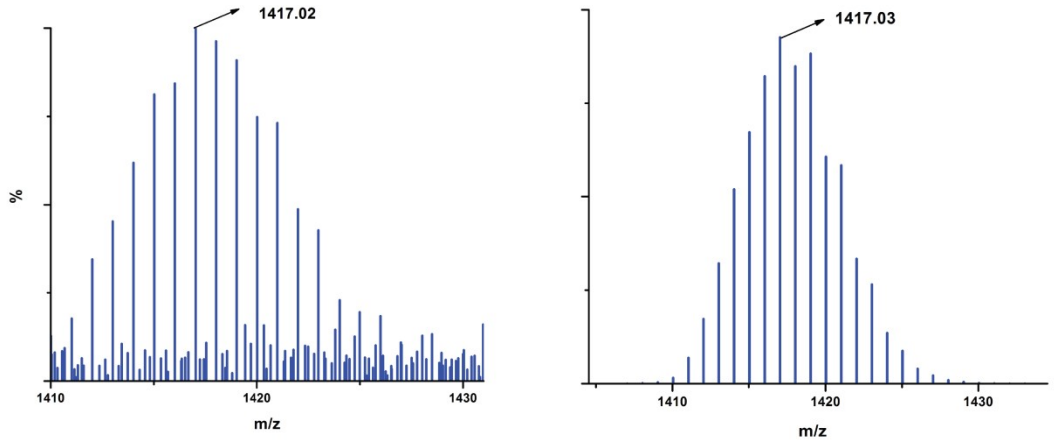

(c) (d)

ESI-MS for complex **2**, detecting $[\{L'_2\{Ni(MeOH)(\mu\text{-}OAc)\}(\mu_3\text{-}MeO)_2Gd_2\}]^+$ fragment, (c) experimental and (d) theoretical.

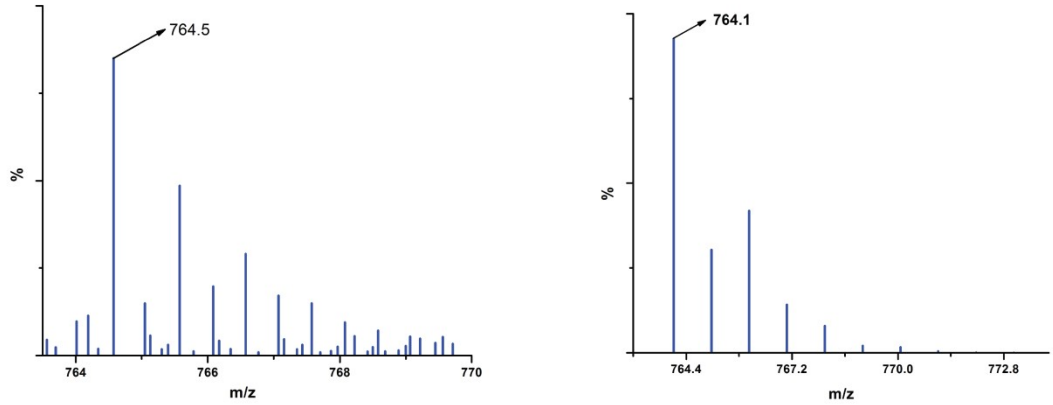

(e) (f)

ESI-MS for complex **3**, detecting $[\{L'\{Ni(MeOH)Tb\}\cdot(H_2O)\cdot(MeCN)_2]^+$ fragment, (e) experimental and (f) theoretical.

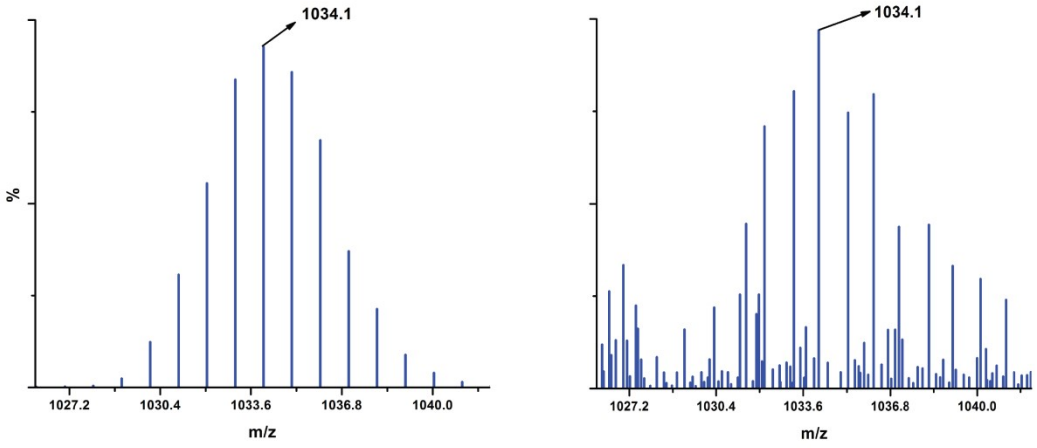

(g) (h)

ESI-MS for complex **4**, detecting [{L′{Ni(MeOH)(μ-OAc)}(μ_3-MeO)$_4$Dy$_2$(H_2O)] fragment, (g) theoretical and (h) experimental.

Figure S5. Mass Spectra of complexes **1**-**4** [(a) and (b) for **1**; (c) and (d) for **2**; (e) and (f) for **3**; (g) and (h) for **4**] collected in methanol-acetonitrile solvent.

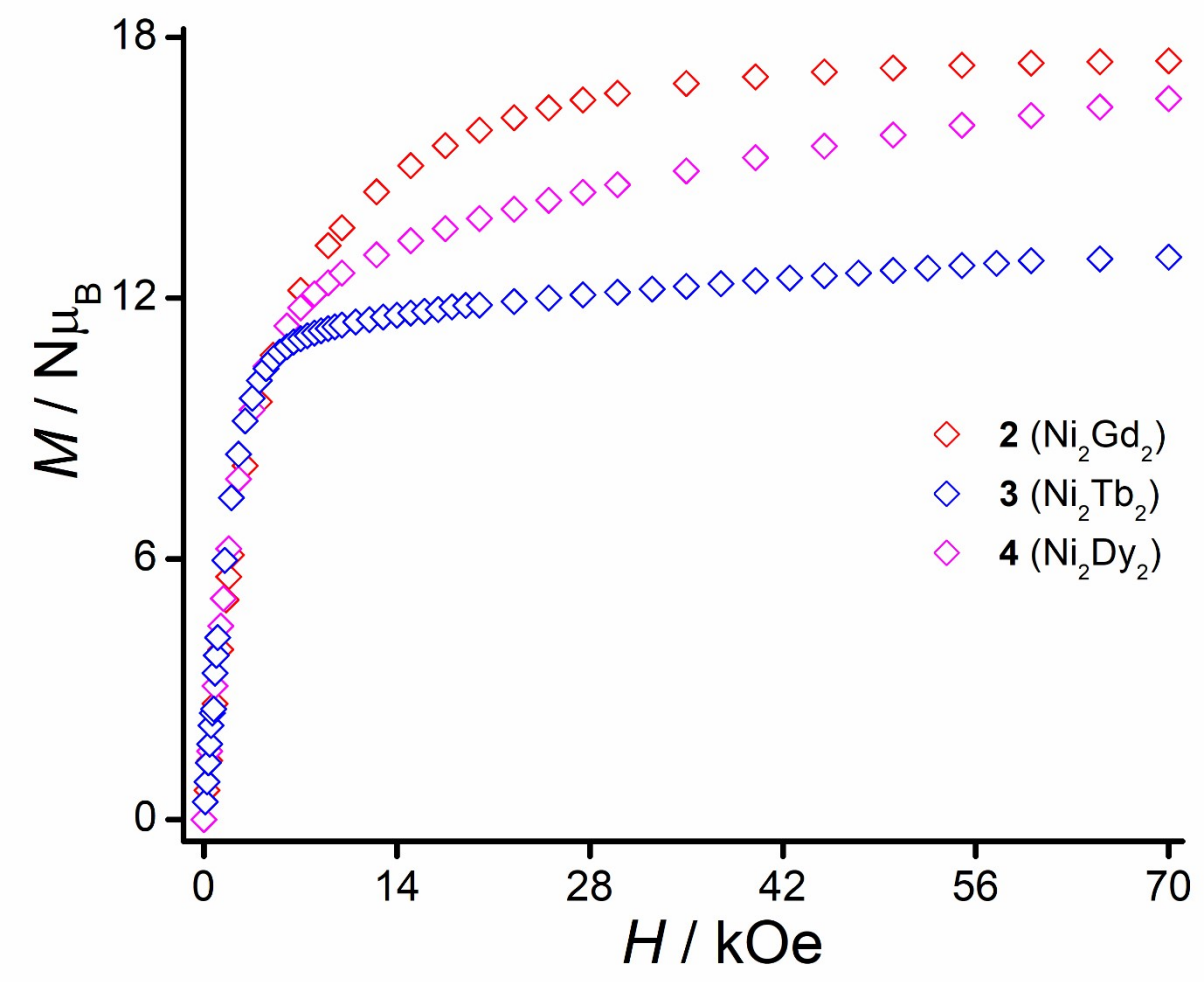

Figure S6. Field dependent magnetization at 1.8 K for complexes **2-4**.

Table S7: Best fitted parameters (χ_∞, χ_0, τ and α) with the generalized Debye model in the temperature range 1.80-2.83 K for complex **3** (H_{dc} = 0 Oe).

T (K)	χ_∞ (cm^3 mol^{-1})	χ_0 (cm^3 mol^{-1})	τ (×10^{-4} s)	α
1.80	22.23707	1.63377	7.148	0.21244
1.89	21.22806	1.82524	5.060	0.20481
1.98	20.17194	2.12911	3.514	0.19399
2.08	19.29892	2.49672	2.625	0.18089
2.20	18.35976	2.95115	1.912	0.16565
2.33	17.39817	3.42789	1.371	0.15010
2.48	16.39003	3.86542	0.9589	0.13343
2.64	15.34065	4.05234	0.6346	0.11797
2.83	14.26437	3.39710	0.3688	0.10925

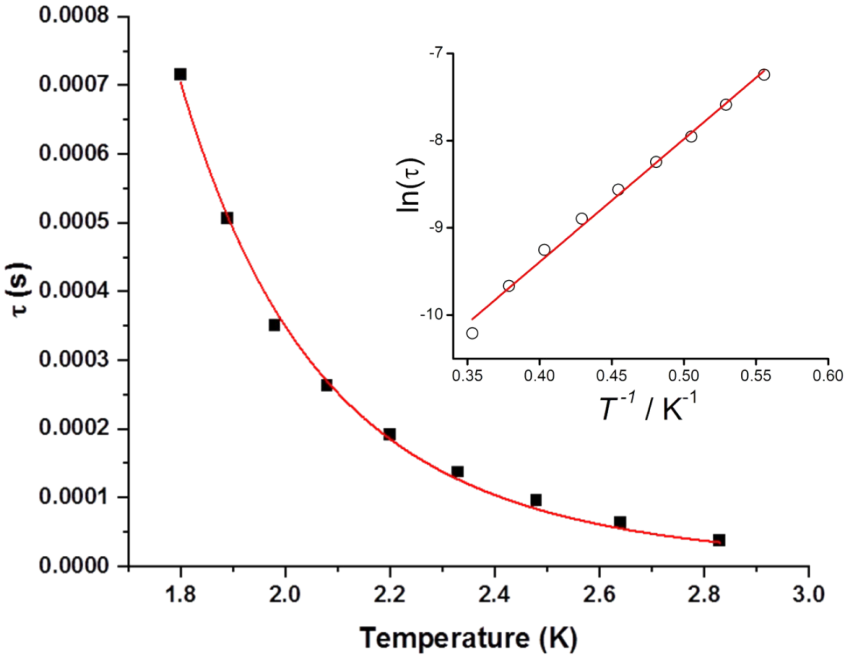

Figure S7. Relaxation times (from zero field measurement) as a function of temperature for complex **3**. Full squares: experimental points, red line: best fit with Raman process. ln(τ) vs 1/T plot fitted by Arrhenius law (inset).

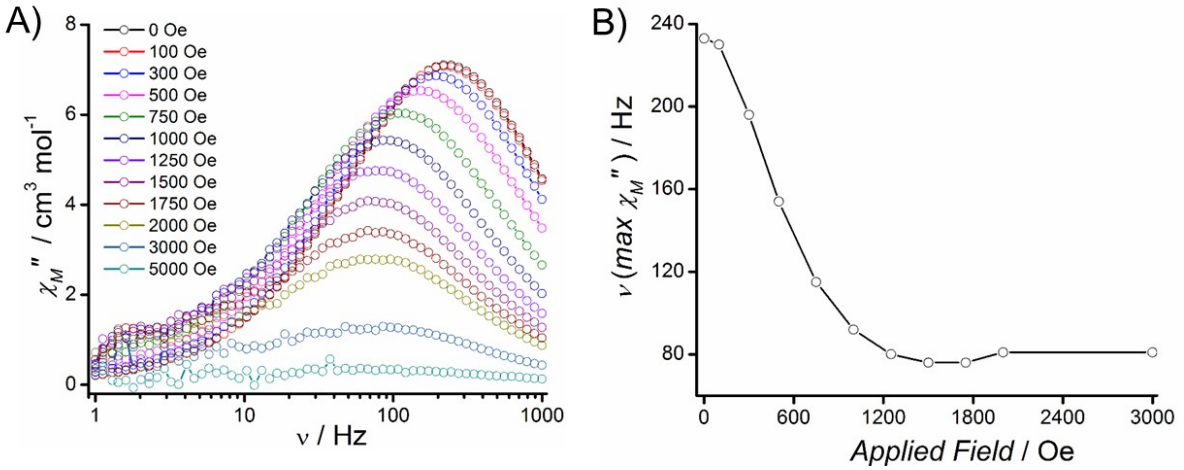

Figure S8. Field dependent ac magnetic susceptibility measurement for complex **3**. A) out-of-phase susceptibility curves for complex Ni_2Tb_2 at 1.8 K with an ac field of 2 *Oe* and under various applied dc fields. B) frequency of the maximum of χ_M'' as a function of the applied dc field.

Supporting Information

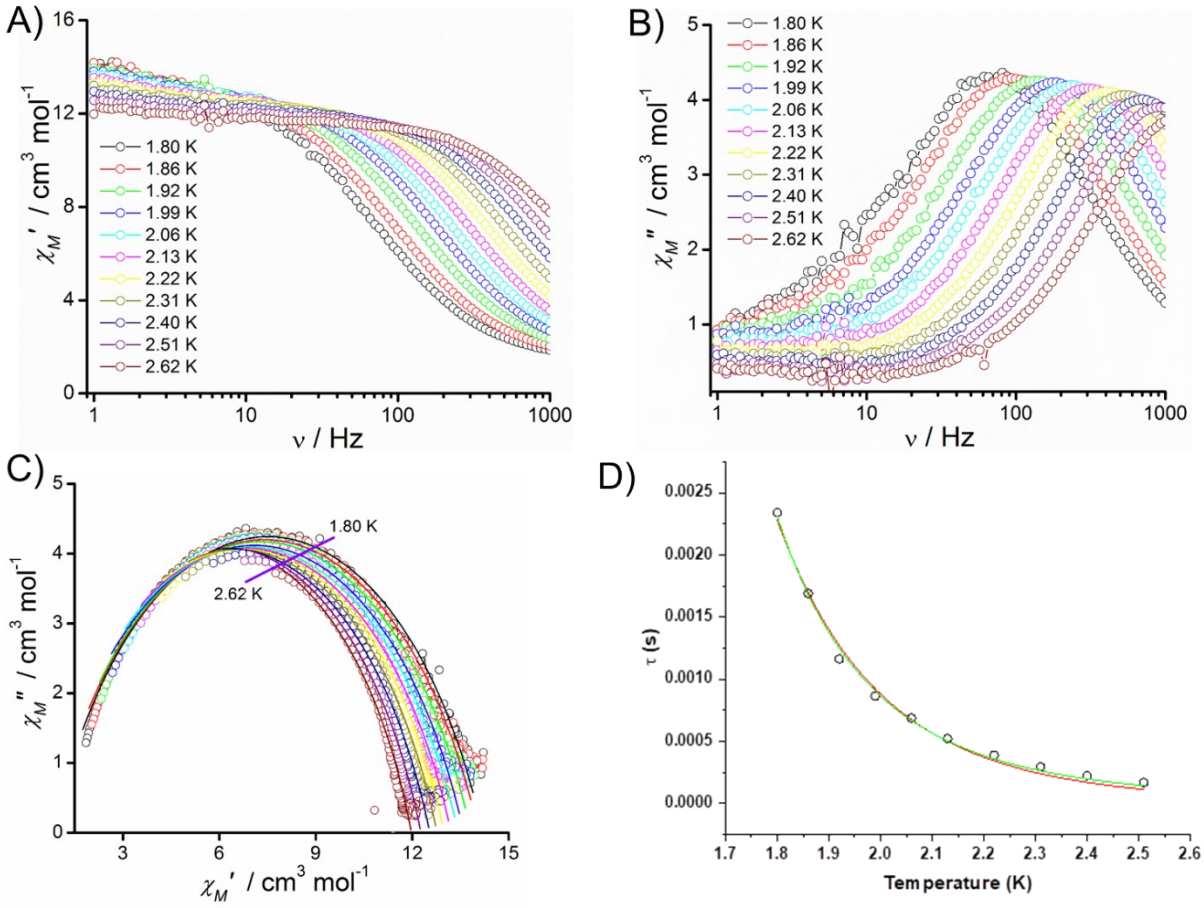

Figure. S9. Ac susceptibility measurement under H_{dc} = 1.5 k*Oe* and H_{ac} = 2 Oe for complex **3**. In-phase (A), out-of-phase (B) susceptibilities and Cole–Cole (C) plots respectively. (D) Best fits of the relaxation times (open circles: experimental points, full red line : best fit using Raman mechanism, full green line : best fit using Orbach mechanism).

Table S8. Best fitted parameters with the generalized Debye model for complex **3** under H_{dc} = 0.15 k*Oe* in the temperature range 1.8-2.62 K.

T (K)	χ_∞ (cm^3 mol^{-1})	χ_0 (cm^3 mol^{-1})	τ ($\times 10^{-4}$ s)	α
1.80	14.19198	0.8319	24.6	0.2797
1.86	14.06964	0.7467	18.1	0.28405
1.92	13.82743	0.73357	12.5	0.27792
1.99	13.6014	0.60761	8.86	0.28085
2.06	13.42961	0.5166	6.61	0.28099
2.13	13.21077	0.47336	4.86	0.27511
2.22	12.99189	0.44575	3.55	0.26792
2.31	12.77427	0.33485	2.56	0.26369
2.40	12.54407	0.09791	1.79	0.26244
2.51	12.27017	0	1.24	0.25504
2.62	11.97271	0	0.89	0.23887

Supporting Information

Table S9. BS-DFT computed energies of high-spin and broken-symmetry solution of complex **2** using H=-JS_1S_2 formalism. Here we have chosen five solutions to extract the J value.

Solution	**Energy (E_h)**	ρ^{Gd1}	ρ^{Gd2}	ρ^{Ni1}	ρ^{Ni2}	$<S^{**2}>$	***J* (cm^{-1})**
HS	-7015.793087	7.015	7.027	1.710	1.710	90.029	J_1 = 1.027
BS1	-7015.793047	-7.024	7.028	1.710	1.710	13.029	J_2 = 0.513
BS2	-7015.793009	7.017	-7.029	1.708	1.708	13.029	J_3 = 0.024
BS3	-7015.792975	7.023	7.029	-1.709	-1.709	34.029	J_4 = 0.324
BS4	-7015.793027	7.019	7.028	1.709	-1.709	58.029	
BS5	-7015.793026	7.020	-7.029	-1.710	1.708	9.029	
BS6	-7015.793026	7.020	-7.029	1.708	-1.710	9.029	
BS7	-7015.793026	-7.020	7.029	1.710	-1.708	9.029	

- *see Figure S10 for J values.*

Table S10. BS-DFT computed energies of high-spin and broken-symmetry solution of complex **1** using H=-JS_1S_2 formalism. Here we have chosen five solutions to extract the J value.

Solution	**Energy (E_h)**	ρ^{Gd1}	ρ^{Gd2}	$<S^{**2}>$	**J**
HS	-6863.888878	1.6794	1.6794	6.0086	-0.273
BS1	-6863.888876	1.6771	-1.6771	2.0086	

J values are estimated using the following equation,

$$J = \frac{E_{BS} - E_{HS}}{s_1 s_2 + s_2/2}$$

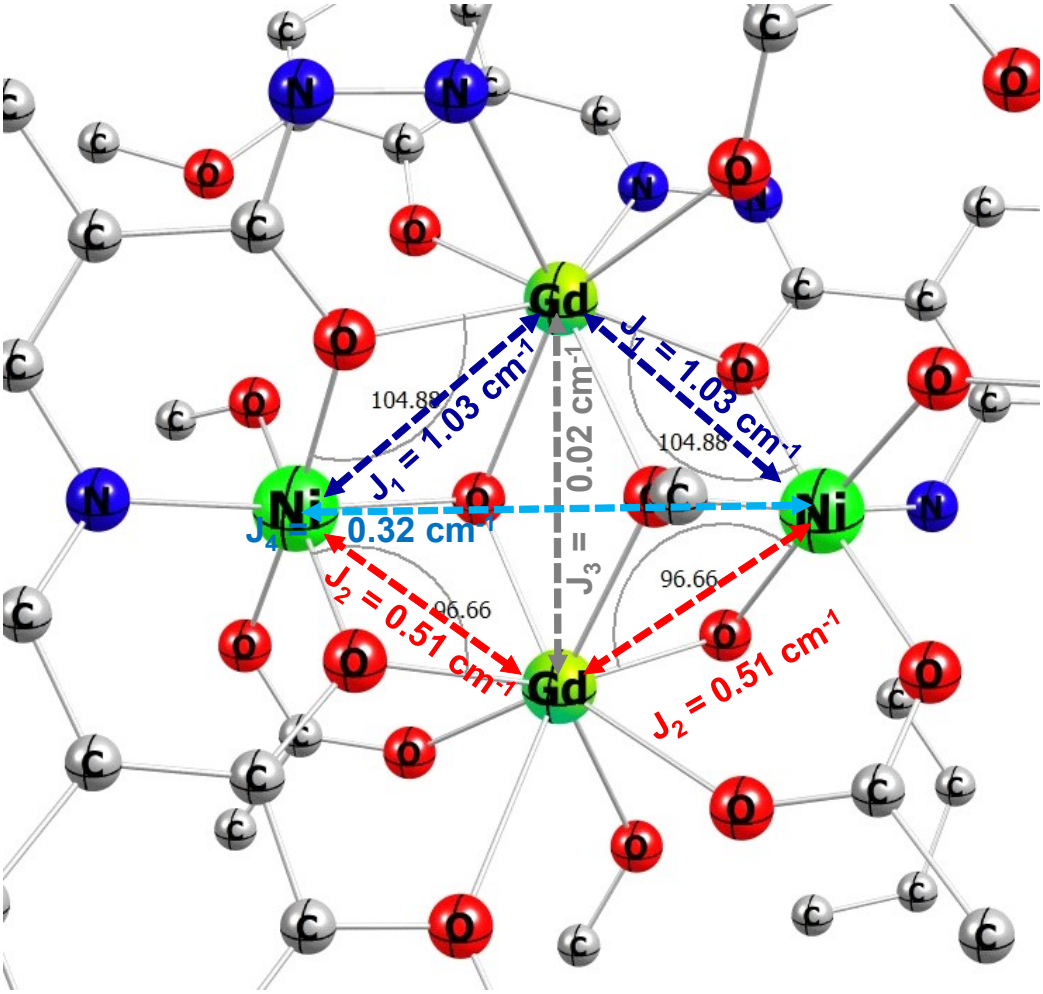

Figure S10. Core structure of complex **2** with relevant ∠Ni-O-Gd bond angle and the corresponding J values.

Supporting Information

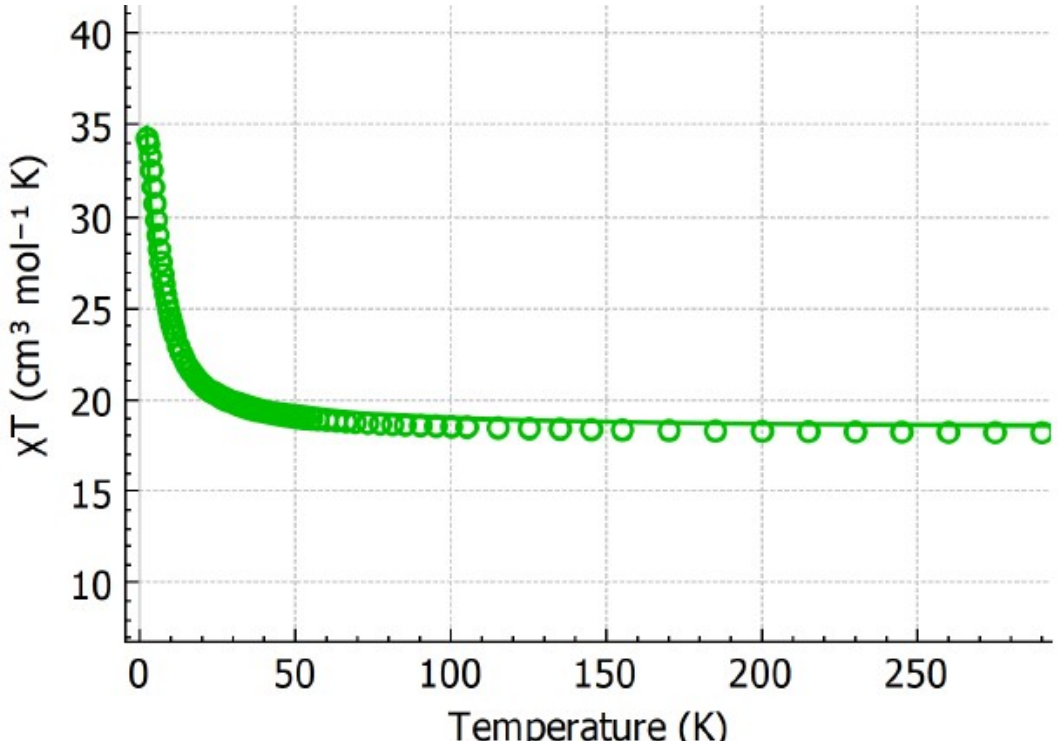

Figure S11. Thermal variation of $\chi_M T$ for complex **2**. The green hollow circle represents the experimental magnetic susceptibility data, while the green curve represents simulation with DFT calculated *J* values. The g-values for Ni(II) centers are 2.28; 2.29; 2.33, while isotropic g-values of 2.0 chosen for Gd(III) center.

Table S11. Calculate overlap integral values for both {NiGd} centers with different bond angles. The values kept in bold format are the strongest overlaps.

Gd1	**∠Ni-O-Gd (96.6°)**		**Gd2**	**∠Ni-O-Gd (104.8°)**	
f-orbital (number)	**Ni(d_{x2-y2}) orbital**	**Ni(d_{z2}-orbital)**	***f-orbital (number)***	**Ni(d_{x2-y2}) orbital**	**Ni(d_{z2}-orbital)**
167	-0.0060	-0.0043	174	**-0.0147**	0.0025
168	0.0042	**-0.0182**	175	**-0.0289**	0.0010
169	0.0032	-0.0047	176	-0.0072	**0.0161**
170	**-0.0118**	0.0090	177	-0.0068	-0.0035
171	0.0054	-0.0046	178	0.0047	-0.0091

172	**0.0106**	0.0086	179	-0.0066	-0.0056
173	**0.0114**	**0.0128**	180	-0.0071	-0.0002

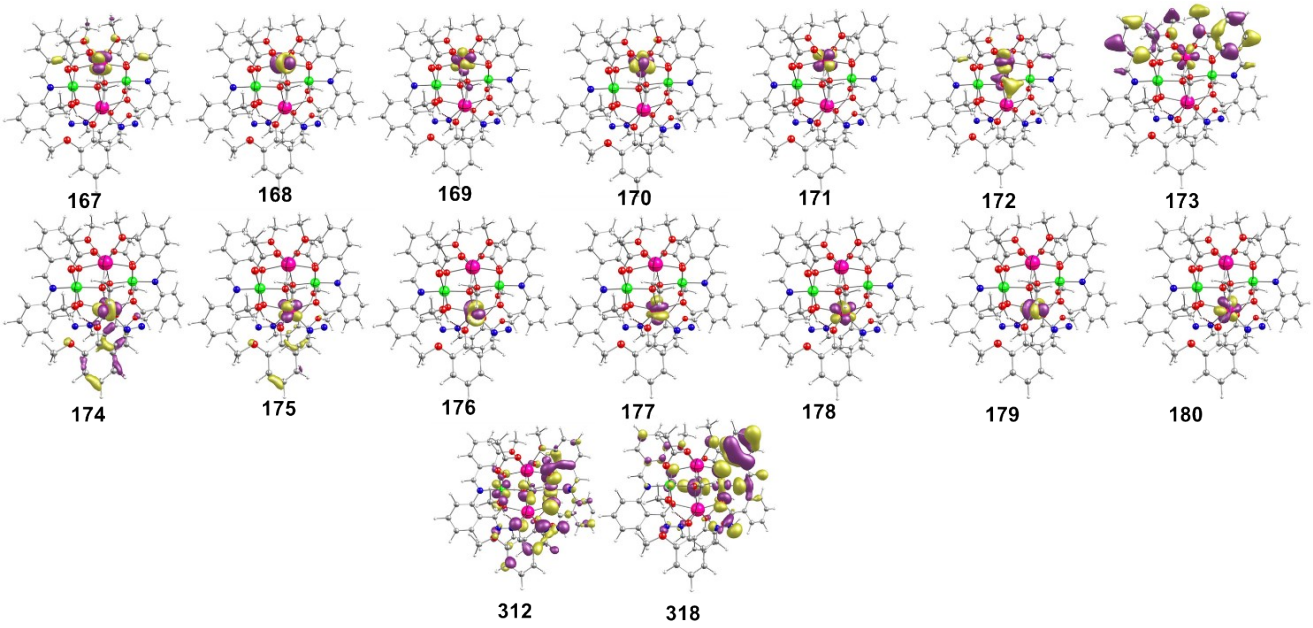

Figure S12. The corresponding orbitals for which the overlap integral values were calculated between {NiGd}centers in complex **2**.

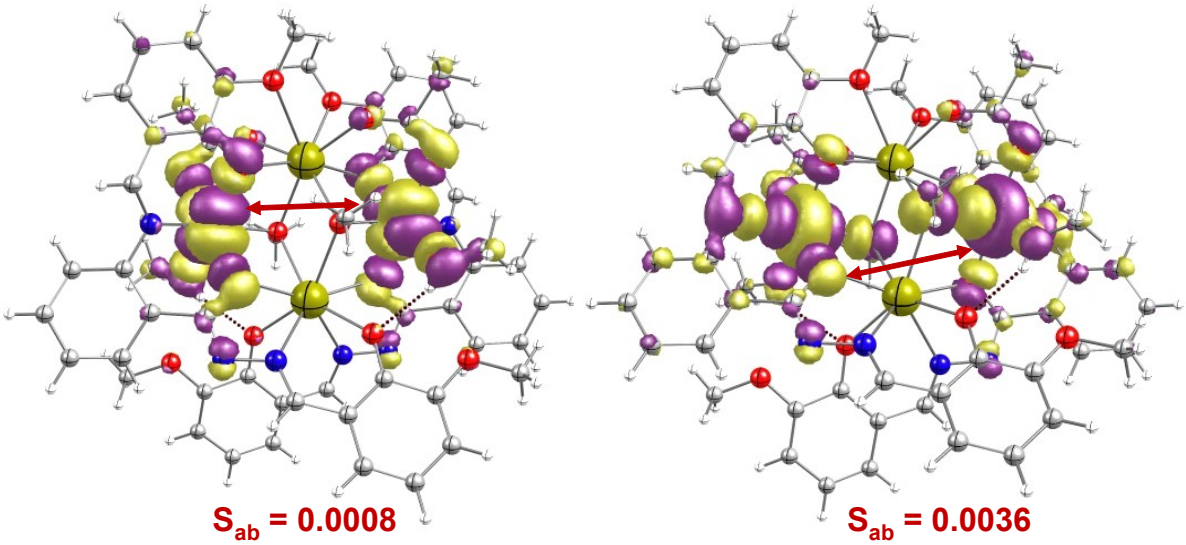

Figure S13. The corresponding orbitals and the computed overlap integral value between the Ni—Ni centers in complex **1**.

Supporting Information

Table S12. Basis functions used in *ab initio* CASSCF calculations using MOLCAS 8.2 code.

Atoms	ANO-RCC basis functions
H	2s
C	3s2p
N, O	3s2p1d
Zn	5s4p2d1f
Ni	6s5p3d2f1g
Y	7s6p4d2f1g
Dy, Tb	8s7p5d3f2g1h

Supporting Information

Table S13. CASSCF computed low-lying 7 septets (grey) and 140 quintets (red) spin-free states for Tb1 and Tb2 centres in complex **3**. All the values are reported here in cm^{-1}.

Spin-free states					
Tb1			**Tb2**		
0.0	40479.4	57927.1	0.000	40382.1	57838.2
117.0	40505.2	58001.0	25.9	40387.0	57894.8
374.0	40516.5	58008.2	166.6	40427.0	57895.3
395.1	40536.0	58110.0	418.1	40442.9	57972.6
769.4	40562.8	58140.1	444.5	40470.4	57980.8
835.1	40632.7	58156.8	685.8	40484.5	58009.1
940.7	40636.2	68685.4	709.8	40485.1	68555.0
25813.7	40678.9	75211.3	25707.0	40542.8	75112.7
25824.6	40687.2	75217.3	25713.3	40574.4	75120.2
25924.3	40739.6	75222.6	25778.0	40580.3	75121.6
26001.6	40776.2	75269.5	25861.0	40635.2	75152.1
26024.6	40820.8	75294.6	25870.1	40644.0	75179.0
29308.2	40826.4	75342.1	29247.5	40691.2	75214.6
29312.1	40873.4	75357.8	29249.5	40734.0	75239.8
29334.5	40925.4	75391.2	29257.4	40765.2	75260.9
29363.0	40937.7	75404.9	29263.5	40767.6	75283.2
29363.0	45897.1	75433.7	29294.7	45769.8	75286.6
29411.8	45905.2	75466.8	29295.6	45774.7	75367.1
29497.1	45955.1	75595.2	29421.8	45833.3	75401.0
29543.4	45959.6	75612.3	29421.9	45834.6	75435.1
29550.3	45965.8	77674.0	29442.0	45843.9	77576.9
29622.4	46009.6	77683.5	29458.1	45875.1	77584.2
29626.0	46023.5	77756.8	29487.0	45905.2	77628.3
29695.3	46044.0	77762.3	29492.1	45909.5	77637.8
29696.1	46067.0	77775.5	29502.4	45910.0	77720.9
29731.3	46091.0	77988.6	29538.7	45974.4	77807.8
29735.0	46130.8	78105.0	29544.8	45997.5	77914.2
29865.7	46140.3	93198.8	29695.6	46013.5	93142.6
29866.8	46180.6	93214.4	29696.6	46024.8	93169.4
30714.8	46256.9	93398.3	30606.2	46097.5	93400.0
30743.4	46265.5	93533.4	30661.5	46097.7	93434.9
30870.5	50249.8	93588.5	30709.1	50159.2	93569.7
30926.7	50269.1	93810.4	30787.8	50182.0	93647.5
30947.5	50274.9	93851.1	30824.8	50191.0	93687.5
30958.8	50353.5	94123.3	30835.5	50200.6	93866.8
30971.2	50358.8	94141.8	30848.7	50226.4	93885.8
31025.6	50380.9	95281.6	30855.8	50235.2	95227.4
31029.0	50403.7	95357.0	30863.5	50267.9	95229.4
35369.3	50513.5	95577.5	35264.4	50370.0	95489.7
35375.3	50528.4	95839.4	35301.3	50385.6	95636.4
35460.9	51828.9	95844.1	35363.0	51734.5	95643.6
35463.4	51898.8		35382.4	51840.5	
35498.1	52114.1		35385.1	51973.7	
35580.8	52264.2		35478.0	52075.2	
35694.6	52339.6		35538.2	52136.3	
35695.8	54667.5		35549.3	54566.1	
35776.3	54815.0		35579.1	54723.5	
35830.6	55040.0		35648.6	54860.4	
35861.4	57812.9		35668.2	57670.0	
40370.2	57859.9		40252.1	57717.9	
40382.9	57864.8		40307.2	57721.8	
40431.1	57899.7		40307.8	57738.0	
40468.4	57909.2		40321.2	57800.2	

Table S14. CASSCF+RASSI-SO computed low-lying spin-orbit states, corresponding g-values and tunnel splitting values for Tb1 and Tb2 centres in complex **3**. All the energy values are reported here in cm^{-1}.

Tb1		
$\pm m_J$ *states*	g_{zz}	Δ_{tun}/cm^{-1}
0.000/0.049	17.6681	0.049
173.4/ 174.4	13.7219	0.990
302.5/ 310.8	9.6761	8.294
448.8/ 473.3	8.5774	24.467
492.9/504.1	11.5530	11.170
640.0/642.0	17.0905	2.0
Tb2		
0.0/ 0.3	17.6415	0.368
113.9/130.0	12.4421	16.125
222.0/225.2	9.2048	3.224
340.5/344.7	13.2076	4.204
426.7/428.1	16.1552	1.400
461.1/463.03	14.4483	1.852

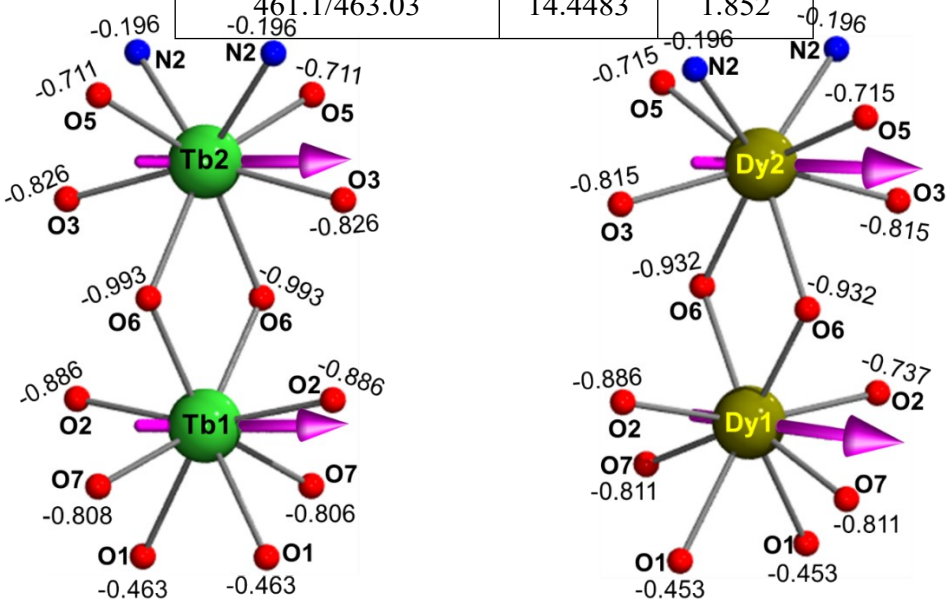

Figure S14. CASSCF computed LoProp charges on the first coordinating atoms of Tb and Dy centers in complex **3** and **4** respectively along with the ground state g_{zz} orientation.

Table S15. SINGLE_ANISO computed wave function decomposition analysis for Tb1 and Tb2 centres in complex **3**. The major dominating values are kept in bold.

Supporting Information

$\pm m_J$	*wave function decomposition analysis*
Tb1	
1	**96.6% |±6⟩** + 2.6% |±4⟩
2	**86.6% |±5⟩** + 8.6% |±3⟩ + 3.6% |±2⟩ + 1.1% |±1⟩
3	**62.0% |±4⟩** + 19.3% |±1⟩ + 13.5% |±2⟩ + 2.4% |±6⟩ + 2.4% |0⟩
4	**38.6% |0⟩** + 37.6% |±3⟩ + 14.3% |±1⟩ + 7.6% |±5⟩ + 1.4% |±4⟩
5	**49.1% |±1⟩** + 44.8% |±2⟩ + 3.2% |±3⟩ + 2.6% |±5⟩
6	**52.9% |±1⟩** + 23.9% |0⟩ + 12.0% |±2⟩ + 10.5% |±4⟩
7	**40.1% |±3⟩** + 19.8% |0⟩ + 14.8% |±2⟩ + 12.6% |±1⟩ + 7.6% |±4⟩
Tb2	
1	**95.7% |±6⟩** + 3.5% |±4⟩
2	**62.2% |±5⟩** + 21.9% |±3⟩ + 10.2% |±1⟩ +4.0% |±2⟩ +1.9% |0⟩
3	**35.4% |±2⟩** + 34.8% |±4⟩ + 13.0% |±1⟩ + 13.0% |0⟩ + 3.1% |±6⟩
4	**32.8% |±5⟩** + 32.0% |±1⟩ + 18.7% |±3⟩ + 15.3% |0⟩
5	**59.3% |±4⟩** + 30.5% |±2⟩ + 4.5% |±1⟩ + 3.5% |0⟩
6	**61.1% |0⟩** + 27.0% |±2⟩ + 8.1% |±1⟩ + 2.0% |±5⟩ +1.4% |±4⟩
7	**58.1% |±3⟩** + 32.0% |±1⟩ + 5.1% |0⟩ + 2.2% |±5⟩ +2.2% |±2⟩

Table S16. SINGLE_ANISO computed crystal field parameters for Tb1 and Tb2 centres in complex **3**. The major dominating values are kept in bold.

Supporting Information

k	q	B_k^q	B_k^q	B_k^q	B_k^q
	Complex 3			**Complex 4**	
		Tb1	**Tb2**	**Dy1**	**Dy2**
2	-2	**-0.11E+02**	**0.11E+02**	**-0.36E+01**	**0.14E+01**
	-1	0.96E+01	**0.19E+02**	**-0.48E+01**	**-0.18E+02**
	0	**-0.19E+02**	**-0.13E+02**	-0.88E+00	-0.42E+00
	2	**-0.17E+02**	0.97E+01	**-0.13E+02**	**0.12E+02**
	1	0.70E+01	-0.89E+01	**0.46E+01**	0.68E+00
4	-4	0.77E+00	**0.15E+01**	0.23E-01	-0.17E+00
	-3	**0.83E+01**	**0.12E+01**	0.41E+00	0.47E-01
	-2	**-0.16E+01**	0.38E+00	0.91E-02	-0.18E+00
	-1	0.39E+00	0.13E+00	-0.93E-01	-0.17E+00
	0	-0.31E+00	-0.26E+00	-0.12E-02	0.66E-03
	1	-0.64E+00	0.11E+00	0.83E-01	0.11E+00
	2	0.10E+01	-0.29E+00	0.25E-01	-0.74E-01
	3	-0.40E+00	0.62E+01	-0.52E+00	0.27E+00
	4	0.35E+00	0.43E+00	0.79E-01	0.16E+00
6	-6	0.33E-01	-0.42E-01	-0.85E-03	0.30E-02
	-5	0.87E-01	0.10E+01	0.54E-02	-0.32E-02
	-4	0.79E-02	-0.28E-01	-0.44E-02	-0.12E-02
	-3	-0.53E+00	-0.11E+00	-0.48E-02	-0.21E-02
	-2	0.24E+00	-0.10E+00	0.27E-02	-0.56E-02
	-1	-0.58E-01	0.13E+00	-0.17E-02	-0.14E-03
	0	0.19E-01	0.12E-01	0.16E-03	-0.24E-03
	1	0.10E+00	0.62E-01	-0.65E-02	0.17E-03
	2	-0.14E+00	0.77E-01	-0.20E-02	-0.22E-02
	3	0.23E-01	-0.62E+00	-0.50E-02	-0.11E-01
	4	0.91E-02	-0.10E-01	0.42E-02	0.10E-02
	5	0.10E+00	-0.11E+01	-0.74E-02	-0.82E-03
	6	0.33E+00	-0.87E-01	0.64E-02	0.78E-02

Supporting Information

Table S17. SINGLE_ANISO computed wavefunction decomposition analysis for Dy1 and Dy2 centres in complex **4**. The major dominating values are kept in bold.

$\pm m_J$	*wave function decomposition analysis*
	Dy1
KD1	**95.3% |±15/2⟩** + 3.3% |±9/2⟩
KD2	**89.7% |±13/2⟩** + 4.4% |±7/2⟩ + 3.1% |±9/2⟩
KD3	**72.2 % |±11/2⟩** + 11.7% |±9/2⟩ + 7.7% |±5/2⟩ + 5.5% |±3/2⟩ + 1.0 % |±13/2⟩
KD4	**42.9% |±7/2⟩** + 31.2% |±9/2⟩ + 14.3% |±1/2⟩ + 4.8% |±11/2⟩ + 3.9% |±5/2⟩+ 2.1% |±3/2⟩
KD5	**40.9% |±5/2⟩** + 20.6% |±3/2⟩ + 18.2% |±9/2⟩ +8.6% |±11/2⟩ + 3.6% |±13/2⟩ + 2.5% |±15/2⟩
KD6	**39.9% |±3/2⟩** + 24.1% |±1/2⟩ + 14.7% |±9/2⟩ + 10.8% |±7/2⟩ + 4.6% |±11/2⟩+3.4% |±5/2⟩
KD7	**55.6% |±1/2⟩** + 14.0% |±5/2⟩ + 12.3% |±7/2⟩ + 11.7% |±3/2⟩ + 3.5 % |±9/2⟩ + 2.1 % |±11/2⟩
KD8	**29% |±5/2⟩** + 24.3% |±7/2⟩ + 19.2% |±3/2⟩ + 14.4% |±9/2⟩ + 6.8% |±11/2⟩ + 2.5% |±13/2⟩
	Dy2
KD1	**95.8 % |±13/2⟩** + 1.1% |±9/2⟩ + 0.9% |±7/2⟩
KD2	**87% |±15/2⟩** + 7.7 % |±11/2⟩ + 1.9% |±7/2⟩ + 1.7% |±9/2⟩ + 0.9% |±13/2⟩
KD3	**73.8 % |±11/2⟩** + 10.4% |±9/2⟩ + 9.0% |±15/2⟩ + 2.5% |±5/2⟩ + 2.1 % |±1/2⟩ + 1.9 % |±3/2⟩
KD4	**37.2 % |±7/2⟩** + 23.5% |±9/2⟩ + 16.9% |±1/2⟩ + 15.9% |±5/2⟩ + 2.9% |±11/2⟩+ 1.9% |±15/2⟩
KD5	**46.5% |±3/2⟩** + 22.3% |±5/2⟩ + 11.5% |±1/2⟩ +9.8% |±9/2⟩ + 8.9% |±11/2⟩
KD6	**33.8 % |±9/2⟩** + 31.6% |±1/2⟩ + 18.9% |±5/2⟩ + 9.3% |±3/2⟩ + 3.5% |±11/2⟩+1.7% |±13/2⟩
KD7	**41.5 % |±7/2⟩** + 15.9% |±1/2⟩ + 15.3% |±9/2⟩ + 13.5% |±3/2⟩ + 10.1 % |±5/2⟩ + 2.4 % |±11/2⟩
KD8	**28.9 % |±5/2⟩** + 27.3% |±3/2⟩ + 21.6% |±1/2⟩ + 17.4% |±7/2⟩ + 4.4% |±9/2⟩

Table S18. CASSCF computed low-lying 21 sextets spin-free and CASSCF+RASSI-SO computed low-lying 16 spin-orbit states for Dy1 and Dy2 centres in complex **4**. All the values are reported here in cm^{-1}.

Dy1		**Dy2**	
Spin-free states	Spin-orbit states	Spin-free states	Spin-orbit states
0.00	0.00	0.00	0.00
29.2	37.9	15.2	28.3
83.9	91.8	15.2	77.0
113.0	126.4	61.9	112.2
126.7	186.2	119.4	139.3
294.4	343.9	146.3	205.6
297.6	412.1	198.6	261.7
434.3	616.9	213.8	525.5
451.7	2987.3	306.5	2983.9
746.0	3050.5	596.4	3040.2
754.1	3131.0	617.5	3076.6
7592.5	3218.7	7523.7	3131.4
7654.0	3264.0	7571.8	3161.9
7675.4	3321.9	7620.2	3236.9
7781.4	3413.9	7664.7	3349.8
7804.4	5583.0	7724.4	5561.9
7917.1		7764.7	
7937.4		7801.5	
34722.7		34722.3	
35118.4		34948.6	
35332.9		35233.3	

Supporting Information

Table S19. SINGLE_ANISO computed g-values and the angle of deviation from ground state g_{zz} orientation of low-lying eight Kramers doublet for Dy1 and Dy2 centres in complex **4**.

Dy1		
$\pm m_J$ *states* (from 21 sextets)	g_{xx}; g_{yy}; g_{zz}	θ (^{o} *angle*)
0.0	0.2711; 0.4646; 19.4909	0
37.9	1.0920; 1.2247; 16.3284	2.3
91.8	1.7509; 2.4556; 13.5933	27.0
126.4	1.6625; 2.3431; 12.6605	50.8
186.2	3.6767; 4.7359; 10.0032	95.3
343.9	0.1163; 0.8720; 11.2841	94.3
412.1	0.3394; 0.7249; 12.8175	89.2
616.9	0.0001; 0.0025; 19.0224	65.2
Dy2		
0.0	0.1464; 0.2623; 17.0718	0
28.4	0.0352; 0.0544; 19.1219	3.0
77.0	1.2246; 1.840; 14.9211	22.3
112.2	0.0946; 3.0390; 13.3048	56.4
139.3	1.1675; 1.2892; 9.3543	13.8
205.6	5.7329; 4.7225; 1.5599	90.0
261.7	1.9581; 6.3553; 11.9465	117.6
525.5	0.0039; 0.0106; 19.6458	101.1

Table S20. CASSCF computed g-tensors and D values for Ni1 and Ni2 sites in complexes **1, 3-4**.

	1		**3**		**4**	
	Ni1	Ni2	Ni1	Ni2	Ni1	Ni2
g_x	2.281	2.280	2.272	2.280	2.269	2.281
g_y	2.295	2.293	2.284	2.293	2.289	2.295
g_z	2.335	2.333	2.330	2.333	2.332	2.332
D	-7.321	-7.509	-7.509	-7.509	-7.280	-7.280
E/D	0.171	0.126	0.126	0.126	0.173	0.173
Energies of three low lying Spin-Orbit states						
	0.000	0.000	0.000	0.000	0.000	0.000
	2.518	1.893	1.893	1.893	2.531	2.531
	8.580	8.456	8.456	8.456	8.547	8.546
g-tensors with pseudo spin = 1/2						
g_x	0.000	0.000	0.000	0.000	0.000	0.000
g_y	0.000	0.000	0.000	0.000	0.000	0.000
g_z	4.6707	4.6661	4.6608	4.6661	4.6655	4.6653

Supporting Information

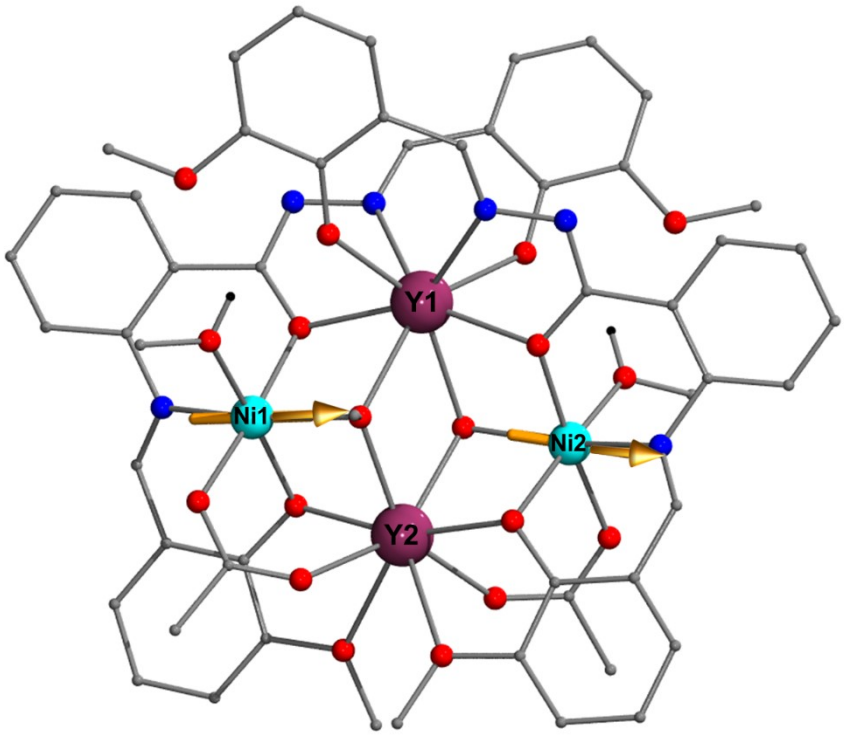

Figure S17. Orientation of D_{zz} axes on Ni1 and Ni2 centers in complex **1**.

Table S21. The exchange spectrum for **3** and for **4** generated from POLY_ANISO simulation of magnetic susceptibility data along with the associated g_{zz} and tunnel splitting (Δ_{tun}) values.

Complex **3**				Complex **4**		
Exchange doublets	**Energy/cm^{-1}**	g_{zz}	Δ_{tun}	**Energy/cm^{-1}**	g_{zz}	Δ_{tun}
1	0.0	44.333	1.8E-05	0.000	41.660	7.3E-05
2	5.718	8.405	3.0E-05	1.717	13.349	4.0E-04
3	9.824	0.259	9.5E-03	4.161	33.969	3.2E-04
4	9.863	0.257	8.1E-03	4.162	13.313	1.2E-04
5	10.218	0.242	9.2E-04	4.379	13.308	4.2E-04
6	10.257	0.240	9.6E-03	4.381	14.064	3.0E-04
7	14.532	8.686	1.1E-05	7.043	27.672	3.3E-04
8	19.910	26.206	1.9E-04	8.322	37.893	1.0E-04
9	116.041	29.543	3.2E-03	9.367	37.893	4.0E-05
10	123.389	0.249	1.7E-02	9.393	37.905	3.7E-05
11	123.434	0.246	2.4E-02	10.367	12.123	8.6E-05
12	130.325	6.422	3.5E-03	10.398	12.133	5.8E-05
13	132.877	23.611	3.5E-03	13.042	12.478	1.2E-04
14	139.741	0.249	2.4E-02	13.049	12.479	5.2E-05
15	139.786	0.247	1.7E-02	13.534	30.850	2.6E-04
16	147.106	11.624	3.2E-03	13.549	30.834	1.8E-04
17	175.461	40.301	5.8E-03	18.760	34.140	5.0E-05
18	180.923	3.029	1.0E-03	19.047	11.079	3.8E-04
19	183.356	0.216	2.0E-01	28.191	44.112	1.6E-06
20	183.690	0.221	1.6E-01	30.066	13.768	4.8E-05
21	184.171	0.207	1.6E-01	32.551	36.849	4.8E-05
22	184.506	0.211	2.0E-01	32.552	36.852	1.3E-05
23	187.065	11.312	8.0E-03	32.824	12.727	5.2E-05
24	192.271	22.240	6.2E-03	32.826	12.726	5.8E-05
25	291.451	25.305	1.0E-01	35.583	12.901	6.4E-05
26	296.857	0.225	7.9E-02	36.910	29.793	2.7E-05
27	297.735	0.224	1.4E-01	37.680	40.223	3.3E-05
28	302.707	2.519	1.1E-01	37.698	40.235	1.8E-06
29	308.268	19.479	1.1E-01	38.075	38.750	1.5E-04
30	313.219	0.225	1.4E-01	38.765	12.178	1.9E-06

31	314.097	0.225	8.0E-02	38.788	12.191	3.3E-05
32	319.484	7.657	1.0E-01	39.561	12.302	1.1E-03

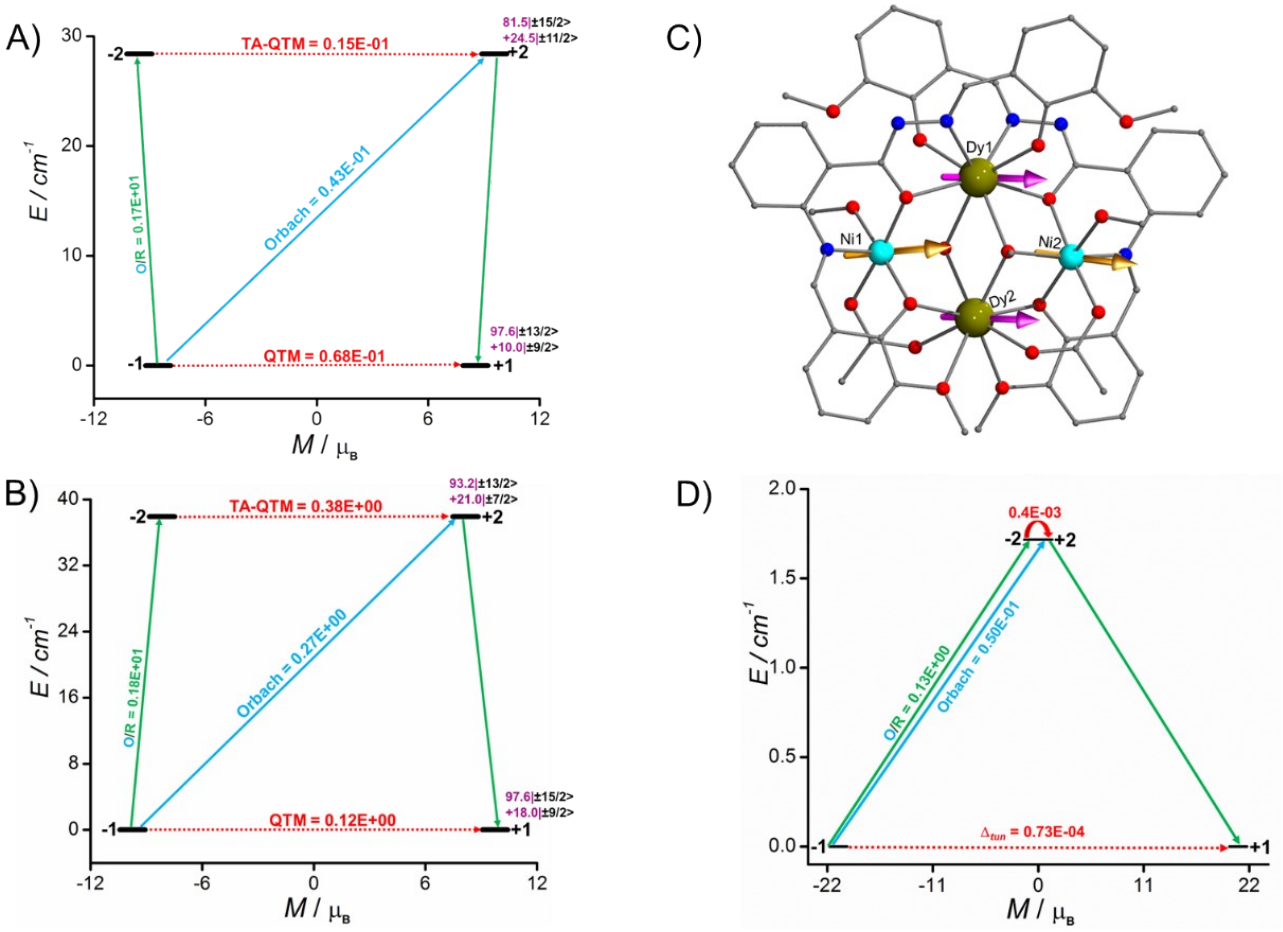

Figure S18. A) SINGLE_ANISO computed ab initio blockade barrier for Dy1 in complex **4**; B) for Dy2 site in complex **4;** C) ab initio computed orientation of ground state anisotropy axis on each of the metal centres; D) exchange states obtained from POLY_ANISO simulation. Energy spectrum are arranged on the diagram according to the associated magnetic moment. Red dotted arrows and numbers represent the possibility of quantum tunnelling between KDs while green and sky blue arrows and numbers represent the possibility of Orbach and Orbach/Raman relaxations.

Supporting Information

X-ray structure analysis of H_3L:

The solid-state structure analysis reveal that H_3L possessed non planar architecture with quinazoline ring (Figure S19).[S1] The hetercyclic quinazoline ring contain one keto group [C9=O3, 1.220(2) Å], hydrazo group [N2-N1, 1.374 (2) Å] linked with o-vanilin, and a sp3-hybridized carbon (C16) linked with 2-hydroxy-3-methoxybenzaldehyde moiety (Figure S19). One of the amine nitrogen (N3) of the hetercyclic quinazoline ring, is attached with proton.[S1]

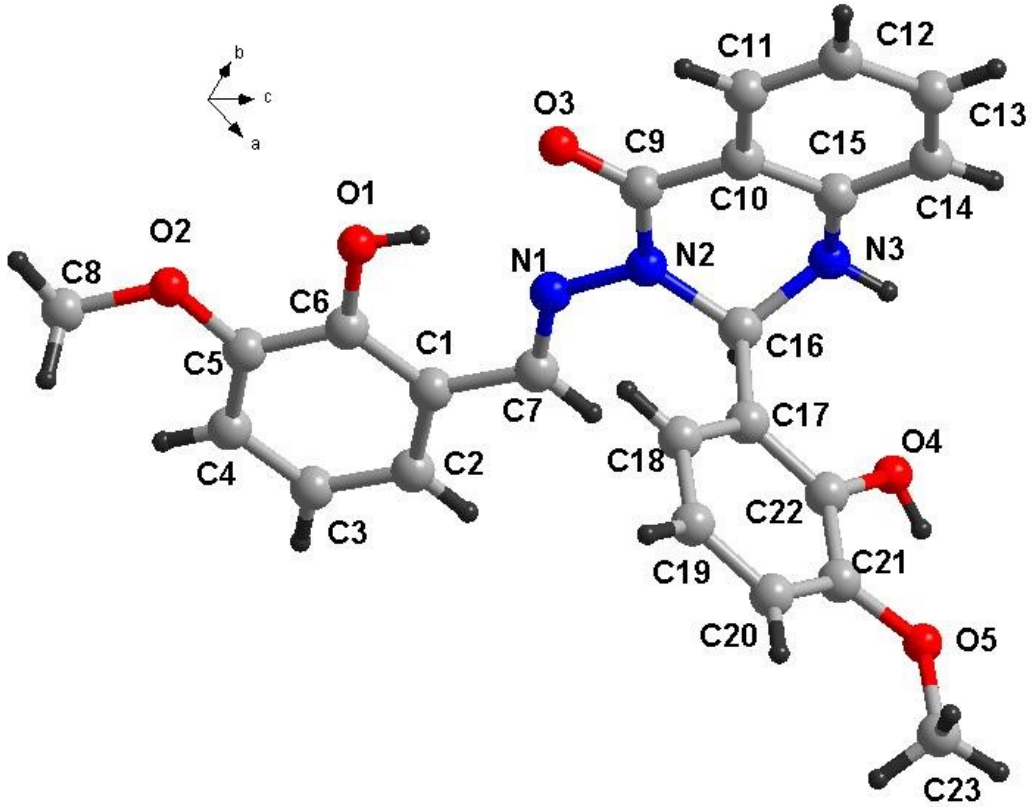

Figure S19. Solid-state molecular structure of H_3L.

References:

S1. K. B. Gudasi, S. A. Patil, R. S. Vadavi, R. V. Shenoy and M. Nethaji, *Transition Met. Chem.,* 2006, **31**, 586.